Impact of the East African Rift System on the routing of the deep water drainage network offshore Tanzania, western Indian Ocean

Citation for published version:
Maselli, V, Kroon, D, Iacopini, D, Wade, BS, Pearson, PN & De Haas, H 2019, 'Impact of the East African Rift System on the routing of the deepwater drainage network offshore Tanzania, western Indian Ocean', *Basin Research*. https://doi.org/10.1111/bre.12398

Digital Object Identifier (DOI):
10.1111/bre.12398

Link:
Link to publication record in Edinburgh Research Explorer

Document Version:
Publisher's PDF, also known as Version of record

Published In:
Basin Research

Basin Research

IAS EAGE

Impact of the East African Rift System on the routing of the deep-water drainage network offshore Tanzania, western Indian Ocean.

Journal:	*Basin Research*
Manuscript ID	BRE-164-2018.R1
Manuscript Type:	Original Article
Date Submitted by the Author:	20-Jun-2019
Complete List of Authors:	Maselli, Vittorio; University of Aberdeen, Department of Geology and Petroleum Geology; Dalhousie University, Department of Earth Sciences, Life Sciences Centre Kroon, Dick; University of Edinburgh School of GeoSciences Iacopini, David; University of Aberdeen, School of Geosciences Pearson, Paul; Cardiff University, School of Earth and Ocean Sciences Wade, Bridget; University College London, Earth Sciences de Haas, Henk; Utrecht University, Royal Netherlands Institute for Sea Research, National Marine Facilities Department
Keywords:	East African Rift System (EARS), Indian Ocean, Davie Ridge, Submarine Canyons, Tanzania, Sediment routing system

Title: Impact of the East African Rift System on the routing of the deep-water drainage network offshore Tanzania, western Indian Ocean.

Authors

Vittorio Maselli[1,2], Dick Kroon[3], David ~~Iacopini[1]~~Iacopini[2], Bridget S. Wade[4], Paul N. Pearson[5], Henk de Haas[6].

Affiliations

[~~2~~1]Department of Earth Sciences, Life Sciences Centre, Dalhousie University~~, 1355 Oxford Street~~, Halifax, Nova Scotia, Canada.

[~~1~~2]School of Geosciences, University of Aberdeen,~~ Meston Bld., King's College,~~ Aberdeen, United Kingdom.

~~[2]Department of Earth Sciences, Life Sciences Centre, Dalhousie University, 1355 Oxford Street, Halifax, Nova Scotia, Canada.~~

[3]School of GeoSciences, University of Edinburgh, Edinburgh, United Kingdom.

[4]Department of Earth Sciences, University College London~~, Gower Street~~, London, United Kingdom.

[5]School of Earth and Ocean Sciences, Cardiff University, Cardiff, United Kingdom.

[6]Royal Netherlands Institute for Sea Research, National Marine Facilities Department and Utrecht University, Netherlands.

Corresponding Author: vittorio.maselli@dal.ca, vittorio.maselli@abdn.ac.uk

Keywords: East African Rift System~~ (EARS)~~, ~~Indian Ocean, ~~Davie Ridge, ~~Submarine Canyons, Drainage~~Sediment routing system, Submarine Canyons, Tanzania, Indian Ocean.

Abstract

The East African Rift Systems (EARS) exerted~~has had~~ a major influence on river drainage basins and ~~the~~ regional climate of east Africa during the Cenozoic. Recent studies have highlighted an offshore branch of the EARS in the western Indian Ocean, where the Kerimbas Graben and the Davie Ridge represent its sea floor expression. ~~However~~To date, a clear picture of the impact and timing of ~~the~~ this EARS offshore branch ~~EARS~~ on ~~the physiography of~~ the continental margin of the western Indian Ocean, and associated sediment dispersal pathways, is still missing~~, and associated sediment dispersal pathways, is still missing~~. ~~T~~This study presents new evidence for four giant ~~and supra-elevated~~ canyons along the northern portion of the Davie Ridge offshore Tanzania. Seismic and multibeam bathymetric data highlight that the southernmost three canyons ~~which~~ are now ~~-~~inactive, supra-elevated relative to~~with~~ the adjacent sea floor of the Kerimbas Graben and disconnected from the modern slope systems offshore the Rovuma and Rufiji River deltas. R~~R~~egional correlation of dated seismic horizons, integrated with well data and sediment samples~~ and high resolution bathymetric data~~, proves that the tectonic activity driving the uplift of the Davie Ridge in this area ~~-~~started ~~in the Plio-Quaternary~~during the middle-upper Miocene and is still active, as suggested by the presence of fault escarpments at the sea floor and by the location and magnitude of recent earthquakes. Our findings contribute to~~in~~ placing the Kerimbas Graben and the Davie Ridge offshore Tanzania in the regional geodynamic context of ~~the~~ the western Indian Ocean and ~~,~~ show how the tectonics of the~~the effect of the~~ offshore branch of the EARS modified the physiography of the margin, re-routing the deep-water drainage network since the middle Miocene. Future studies are needed to understand the influence of changing sea floor topography on the western Indian Ocean circulation~~on sediment distribution pathways,~~ and to evaluate the potential of the EARS

~~underline the need of considering the~~ offshore tectonics ~~activity~~ in generating tsunamigenic events~~in future tsunami hazards assessments in East Africa~~.

1. Introduction

Tectonics exerts an overarching control on the evolution of terrestrial and marine ~~topography~~landscapes, mainly through the modification of ~~surface~~ the topographic relief (Leeder and Jackson, 1993; Schumm et al., 2000). In the last decades, a huge effort has increased our understanding of geodynamic processes leading to the onset of the East African Rift Systems (EARS; ~~(~~Ebinger and Sleep, 1998; Moucha and Forte, 2011 and references therein). However, there is very little knowledge of the links between the Neogene ~~EARS~~ tectonics of the EARS and the development of structural features in the western Indian Ocean.

The timing of the iInitiation of the EARS ~~can be trace~~, datesd backd ~~back~~ to the ~~an~~ Oligocene (Macgregor, 2015, and references therein)., The origin of the EARS has been related to ~~, when~~ the onset of a mantle plume, which generated a topographic anomaly beneath the Ethiopian and East Africa plateaux ~~(Ebinger and Sleep, 1998) generated a topographic anomaly~~(Ebinger and Sleep, 1998).~~ referred to as the EARS.~~ Normal faulting and regional uplift associated with the EARS exerted a major control on the ~~evolution~~ development of the drainage basins of large African rivers, such as the Congo, Nile and Zambesi (Goudie, 2005; Stankiewicz and de Wit, 2006; Roberts et al., 2012), and on the formation of rift lakes (Cohen et al., 1993; ~~MacGregor~~Macgregor, 2015). After the seminal work of Mougenot et al. (1986), a recent study by Franke et al. (2015) highlighted the stratigraphy and architecture of the offshore branch of EARS in the western ~~Somali~~ Indian Ocean~~Basin~~ offshore Mozambique~~,~~. Here, the rift consists of o,a juvenile fault zone at about 17° S, and of the Lacerda half-graben and the southern part of the Kerimbas graben up to ca. 10° S ~~following previous results using remote sensing data, earthquakes distribution and focal mechanisms~~ (Franke et al., 2015)~~, and references therein)~~.. Farther north, offshore of Tanzania, the EARS stretches along the northern part of Kerimbas Graben, which is characterized by a well-developed N-S trending depression bordered by normal faults and confined on its eastern side by the Davie Ridge (Fig. 1). Although the effects of EARS in modifying subaerial landscapes, and its consequence ~~on~~on the evolution of early hominids~~humans~~ ~~evolution~~ and atmospheric circulation, have been ~~investigated~~ established (Sepulchre et al., 2006; Maslin et al., 2014), the control of EARS on location and shape of the deep-water drainage network ~~have~~ has not been investigated~~researched~~, and a clear picture of the evolution of the western Indian Ocean is still missing.

~~Our~~ This contribution presents the discovery of four giant deep-water canyons (up to 15 km wide and up to 850 m deep in water depths >2,500 m~~xxxwidth xxx depth~~), herein named C-1 to C-4 from north to south, incising the Davie Ridge and of which three (C-2 to C-4) are currently disconnected from the active slope channels offshore the Rovuma and Rufiji River deltas. The three canyons~~se~~ appear to be relict features corroborating the existence of an older drainage network that was destroyed by ~~recent~~ the tectonic activity associated with the offshore branch of EARS. Our findings reveal how EARS affected the physiography of the western Indian Ocean, resulting in the formation of a new sediment routing system, and provide~~s~~ new insights in the chronology and ~~outbuilding~~ architectural features of the margin.

2~~3~~. Geological setting

The history of the ~~W~~western Indian Ocean can be traced back to the Early Jurassic, when the onset of rifting occurred between Madagascar and Africa (Revees and de Wit, 2000; Revees et al., 2016). Sea floor spreading started in the Middle Jurassic and continued until the Early Cretaceous (Coffin and Rabinowitz, 1992), leading to the southward drift of Madagascar along the dextral strike-slip structures of the Davie Fracture (or at least along part of it, see below and discussion in Klimke and Franke, 2016) and the Lebombo-Explora Fracture Zones (Revees and de Wit, 2000). From the Cretaceous to the Paleogene (mid-Oligocene), the East African margin was characterized by a period of stability and thermal subsidence (Kent et al., 1971; Salman and Abdula,~~;~~ 1995), which was recorded by deposition of the Kilwa Group in Tanzania (Nicholas et al., 2006; 2007). The passive margin phase was interrupted by a period of neo-rifting and tectonic reactivation: the onset of new mantle circulation beneath the African continent (Ebinger and Sleep; 1998; Moucha and Forte, 2011), known as the African super-swell (Nyblade and Robinson, 1994), evolved into the EARS (Chorowitz, 2005), with synchronous initiation along its western and eastern branches (Roberts et al., 2012). Normal faulting and rifting w~~as~~ere widespread along the Tanzanian margin during the Miocene, promoting the formation of topographic highs, such as Zanzibar, Pemba and Mafia Islands, and lows, such as the coastal basins and the Kerimbas Graben (Kent et al., 1971; Mougenot et al., 1986). Recent studies, however, highlighted the presence of folding and inversion structures on a seismic profile across the channel north of Zanzibar Island (Sii and Underhill, 2015), suggesting that the islands are compressional features associated with fault reactivation and basin inversion.

~~3~~2.1. Kerimbas Graben and Davie Ridge in the offshore of Tanzania

The EARS consists of a series of tectonic basins bordered by uplifted shoulders, which extend for thousands of kilometres along two main lineaments, called the western and eastern branches (Chorowitz, 2005). The continuation of the eastern branch offshore of Tanzania can be traced along the Pemba and Mafia basins, while farther to the south it runs~~ and~~ along the Kerimbas and ~~Lucerna~~Lacerda ~~G~~grabens (Fig. 1), until ending in a juvenile fault zone at about 17° S~~ further to the south~~, in the offshore Mozambique (~~Fig. 1; ~~Mougenot et al., 1988; Franke et al., 2015).

The Kerimbas Graben was firstly recognised by Mougenot et al. (1988) north of the Saint-Lazare Seamount (Fig. 1). A compilation of recently acquired multibeam data (Dorschel et al., 2018) highlight that the graben, north of~~ a~~ 12° S, can be divided in ~~three~~four zones based on sea floor morphology and water depth (Fig. ~~Figs. 1 and ~~2). In zone ~~The southern part (zone ~~1, which extends from the ~~; Fig. 2), between the ~~Saint-Lazare Seamount up to 11.5° S (Fig. 2), the graben is asymmetric, with the western side running along the base of the slope of the northern Mozambique margin and gently dipping at ca. 0.7° to the east, whereas the eastern flank corresponds to a 12° west-dipping fault escarpment (Fig. 2, blue arrow). The sea floor eastward of the escarpment shows a series of morphological steps related to N-S trending faults before gently dipping towards the Indian Ocean (Fig. 2). In zone 2, between 11.5° S and 10°~~ 20'~~ S, the Kerimbas ~~S, ~~is a 30-40 km wide symmetric graben bounded by ca. 15° steep flanks (Fig. 2, green and red arrows)~~,~~. N-S trending lineaments, representing fault escarpments, are visible at the ~~flat ~~sea floor,~~,~~ which ~~ and it shows a flat floor lying ~~lies at an average water ~~maximum ~~depth of ca. 2,900 m and~~,~~ gently dip~~ping~~s to the north (Figs. ~~ 1, ~~2). The western side of the ~~basin~~graben runs along the base of the slope in the offshore Rovuma River delta, whereas~~ while~~ the eastern side corresponds to the Davie Ridge (Fig. ~~1~~2). A series of channels and gullies cut the western flank and are visible on the sea floor (Figs.

1, ~~, 1~~2). The ~~second~~third ~~z~~ zone, located just offshore the Rovuma River between at 10° S (Fig. 2), corresponds to a bathymetric sill with a maximum water depth of ca. 2,750 m (Fig. 2)~~, located just offshore the main Rovuma Channel between 10° 20' S and 9° 05' S (Fig. 1)~~. ;Here, ~~and it is lying at ca. 2,750 metres of water depth (Fig. 2). In this area,~~ the Kerimbas ~~g~~Graben shows asymmetric flanks, with a gentler western side up to 1.5° and a 12° dipping eastern side. In ~~the third~~ zone 4, reaching approximately 8.5° ~~40'~~ S, the graben shows a different morphology with a maximum water depth up to ca. 3,500 me~~tres~~ and a maximum width up to 90 km (Figs. 1, 2). In this area, the western flank of the graben partially corresponds to a structural high (the -Seagap Ridge) generated by the ~~movement~~ tectonics of the Seagap transform fault ~~Seagap Ridge~~ (Fig. 2; Revees et al., 2016), while the western side corresponds to the northern termination of the Davie~~s~~ Ridge (Fig. 2~~1~~). A series of arcuate steps are visible on the sea floor of the graben, likely associated to normal faults developing at the base of the Davie Ridge (see supplementary Figure S1).

The Davie Ridge appears as a bathymetric high roughly extending N-S that dissects the continental slope in the offshore East Africa for more than 1,000 km south of 9° S (Mahanjane, 2014; Courgeon et al., 2018). The ~~ridge shows different~~ maximum elevation of the Davie Ridge~~s~~ (calculated as the depth difference between the top of the ridge and the floor of the Kerimbas Graben along a section, see Figs. 1 and -2) shows ~~in the different zones described above (Fig. 2), with~~ an overall decrease in elevation to the north (Fig. 2). Heirtzler and Burroughs (1971) ~~when discovering the~~firstly described the Davie Ridge ~~described it~~ as a *ridge-like feature*, asymmetric, with a steep western flank (up to 30°) and a gently dipping eastern flank (ca. 0.65° in the offshore Rovuma delta; Fig. 1). Heirtzler and Burroughs (1971) interpreted the ridge as a transform fault resulting from the southward drift of Madagascar relative to the African continent. The continuation of the Davie Ridge north of 9° S, where the ridge does not have a prominent morphological expression on the sea floor (Fig. 1), has been derived by gravimetric and magnetic data showing a series of anomalies, up to 2.5° S (Rabinowitz, 1971; Scrutton, 1978; Coffin and Rabinowitz, 1987). The entire lineament, extending from ca. 20° S to 2.5° S, named the *Davie Fracture Zone* by Scrutton (1978), was interpreted as the bathymetric expression of the transform fault that accommodated southward drift of Madagascar (Scrutton, 1978). A recent study from Klimke and Franke (2016), however, argued the existence of a transform fault extending from northern Mozambique up to Kenya and interpreted the Davie Ridge visible on the bathymetry between 15° S and 9° S (on the eastern side of the Lacerda and Kerimbas grabens) as a rift-flank uplift, originated during the Neogene and probably correlated with the evolution of the EARS in the offshore domain. This interpretation is in agreement with GPS vector data (Calais et al., 2006), and focal mechanisms of recorded earthquakes, showing pure normal faulting with N-NW trending nodal planes and roughly E-W extensional failure (Grimison and Chen, 1988; Yang and Chen, 2010).

32. Data and Methods

32.1. 2D Seismic data

The present study uses two seismic datasets: (1) the GLOW survey (Paleogene GLObal Warming events, GLOW Cruise; Kroon and the Shipboard Scientific Party, 2010) performed onboard of the R/V Pelagia in 2009 and consisting of 2,450 km of seismic lines; and (2) the multi-client 2D seismic dataset Tanzania, acquired by WesternGeco-Schlumberger in 1999-2000 and consisting of 5,550 km of seismic lines.

The GLOW seismic survey was performed using an array of four airgun sources (10, 20, and 2× 40 in^3) and a 24-channel streamer as a receiver. The seismic data were recorded using the GeoResources Geo-Trace 24 system. The peak frequency of the combined signal of the guns is within the range of 50-150 Hz, with lower amplitude frequencies up to 400 Hz. The guns were towed in a frame at a depth of 1.7 metres, 42 metres behind the stern of the ship, and fired every 10 seconds at a pressure of 115 bars. The average sailing speed was 4.2 knots thatwhich resulted in an average distance between the shots of 21 metres. The streamer consisted of four 63 m long active sections with 6 channels each (channel interval 10.5 metres). Each channel consists of ten 1-m-spaced Teledyne T2 hydrophones. The streamer is ended by a 0.5 m tail-end, which contains the last terminating end connector. The receiver was attached to the ship by a tow leader of 60 m and a stretch member of 25 m. The streamer was towed at a depth of 1 metre below the surface. Three (front, mid, end) I/O systems 5010 DigiBIRDS were used to keep the streamer at depth. During the recording of line 2 one bird failed. From line 3 onwards only 2 birds (front, end) were used. This had no noticeable effect on the streamer position. The record length was 7,500 ms (including the water column) and the sampling rate was 2 kHz for the first lines. From line 5 onwards the sampling rate was 1 kHz. The data were recorded with a 10 Hz high pass filter. The vertical resolution of the seismic data in the investigated section ranges between 2.5 and 5 metres, calculated considering a peak frequency of 150-200 Hz and interval velocities of 1,800-2,900 msec^{-1}.

Processing of the data was performed at NIOZ by means of the software package RadexPro (DECO Geophysical, Moscow). The processing sequence included data loading, 30-700 Hz bandpass filtering, amplitude correction, an interactive velocity analysis, NMO correction, 6 fold CDP-stacking, Stolt F-K migration and water column muting.The present study uses two seismic datasets: (1) a seismic survey (Paleogene

GLObal Warming events, 'GLOW' Cruise, Kroon and the Shipboard Scientific Party, 2010) performed on board of the RV Pelagia in 2009 consisting of 2,450 km of seismic lines, and (2) the multi-client 2D seismic dataset Tanzania, acquired by WesternGeco-Schlumberger in 1999-2000 consisting of 5,550 km of seismic lines.

The GLOW seismic survey was performed carried using three3 airgun s sources (of 20, 30 and 40 incubic inch3) each as a source and a 24-channel streamer as a receiver. The streamer consisteds of four 63 m long active sections with 6 channels each, and the seismic data were recorded. Data recording was performed using the Geo-Resources Marine MultiGeo-Trace 24 hard- and software. The system has a 24 channel digital pre-amplification system and 24 channel bandpass filter already integrated. The record length was 7,500 ms (including the water column) and , the sampling rate was 2 kHz. The data were recorded with a 10 Hz high pass filter. Processing of the data was performed at NIOZ by means of the software package RadexPro (DECO Geophysical, Moscow). The processing sequence included data loading, 30-700 Hz bandpass filtering, amplitude correction, an interactive velocity analysis, NMO correction, CDP-stacking, Stolt F-K migration and water column muting.

The 2D survey offshore Tanzania was shot by Western-Ggecophysical using a 5,200-m-long streamer length andwith hydrophones at a 12.5 m receiver interval. In 2012, the legacy 2D was reprocessed by WesternGeco using Anisotropic Kirchoff pre-stack Time time Mmigration (add ref), to obtain an improved signal resolution. One of the key processing challenges was represented by the presence of strong sea-bed multiples and inter-bed multiples. The reprocessed 2D seismic lines has produced an overall better overall reflection detail, -enhanced data resolution, and improved fault definitions and events continuity, thus which providinges much higher confidence during interpretation of geological features. The vertical resolution of the seismic data in the investigated section ranges between 7 and 14 metres, calculated considering a peak frequency of 50-60 Hz and interval velocities of 1,800-2,900 $msec^{-1}$.

A post-stack seismic attribute, the~~Seismic attributes were generated for helping interpretation. In particular, the r~~ root-mean-square (RMS) ~~seismic~~ amplitude, was used to support the interpretation. In detail, the RMS, which ~~which~~ represents the square root of the arithmetic mean of the squares of the seismic amplitudes within a defined window interval, helped~~were used~~ to unravel the presence of coarse-grained facies (Rijks and Jauffred, 1991; Chen and Sidney, 1997; Brown, 2004).

Additional data used in this study include the multichannel seismic profiles acquired during the R/V VEMA cruises 3618 and 3619 (Coffin and Rabinowitz, 1982), and available through the Marine Geoscience Data System (http://www.marine-geo.org/index.php), and published seismic profiles (Mougenot et al., 1986; Franke et al., 2015).

~~Three seismic horizons, named H1 to H3, and associated seismic sequences (S1 to S4), were identified based on seismic facies and reflector terminations, mapped throughout the study area, and integrated with all the data available in literature in order to develop a chronological framework for the Davie Ridge.~~

3~~2~~.2. Multibeam ~~Echosounder~~ echosounder data

During the GLOW survey, ~~Multibeam surve~~bathymetric~~ys~~ data were collected~~carried out~~ with a~~with the~~ Kong~~g~~sberg EM302 multibeam echosounder, permanently installed on board the R/V Pelagia. The maximum swath opening angle ~~is~~ was 150 degrees. The transmitter array ha~~s~~d a beam opening angle of 1 degree while the receiver array had~~s~~ a beam opening angle of 2 degrees. These arrays ~~are~~ were connected to a transceiver unit (TRU). The TRU received~~s~~ ~~the ships attitude (~~corrections for heave, roll~~,~~ and pitch ~~and heading,)~~ from a Kongsberg MRU5 motion sensor. A Seapath200 served~~s~~ as positioning and heading system ~~and also sends its data to the TRU.~~. The sound velocity in the water column was ~~is~~ determined from a salinity/temperature CTD deployment and calculated using the Chen-Millero formula (Chen and Millero, 1977). ~~Processing of the~~ D~~d~~ata Processing was~~as~~ performed using the Neptune ~~-~~(Kongsberg) and Fledermaus (QPS) software packages. The data were presented as a 100 × ~~x~~ 100 m surface grid, ~~that has been~~and integrated with the Southwest Indian Ocean Bathymetric Compilation (swIOBC; Dorschel et al., 2018), available at a 250 m horizontal resolution.

3~~2~~.3. Sediment samples

Short seabed samples were collected during the GLOW cruise using a NIOZ designed box corer with a ~~. The box core has a barrel with a~~ diameter of 30 cm and a height of 55 cm. The box corer was~~is~~ supplied with a lid that closes the box from the top as soon as it ~~has~~ penetrated the sediment. This configuration avoided the ~~In this way~~ sloshing of ~~the~~ water above the sediment surface ~~is avoided when t~~during the recovery~~he core is retrieved and hoisted on deck~~, resulting in an undisturbed sample of the seabed surface sediments. On deck the bottom water was siphoned off and the surface sediments were described and photographed. Four plastic liners were inserted and retrieved from the core. These subsamples were stored at a temperature of 4° C. A key objective of the GLOW survey was to take sediment cores where fossil stratigraphic layers crop out at the sea floor in order to provide age control on seismic reflectors. This occurred on flanks of submarine channels (see supplementary material). Samples were washed over a 63 micron sieve and dried at 40° C in an oven. Washed residues were studied for index fossils, and biostratigraphic age assignments were made ~~using~~ following Wade et al. (2011).

3.4. Well data

Eight exploration wells (Fig. 1) with check-shots, velocity models, and biostratigraphic information were made available for this study by Royal Dutch Shell and Shell Tanzania. The wells were tied to specific~~the~~ seismic reflectors ~~-~~allowing the age determination of the seismic horizons.~~ascorrelating specific reflectors to~~

~~**3. Geological setting**~~

~~*3.5. Seismic interpretation*~~

~~Three seismic horizons, named H1 to H3, and associated seismic sequences, were identified based on seismic facies and reflector terminations and mapped throughout the study area. In detail, the three sequences, named S1 to S3 from deep to shallow, show diagnostic seismic facies, reflection geometries, and RMS amplitude values. Sequence S2 was further subdivided in two units (named S2a and S2b) by horizon J (Figs. 3, 4).~~

~~The history of the Western Indian Ocean can be traced back to the Early Jurassic, when the onset of rifting occurred between Madagascar and Africa (Revees and de Wit, 2000; Revees et al., 2016). Sea floor spreading started in the Middle Jurassic and continued until the Early Cretaceous (Coffin and Rabinowitz, 1992), leading to the southward drift of Madagascar along the dextral strike-slip structures of the Davie Fracture (or at least along part of it, see below and discussion in Klimke and Franke, 2016) and the~~

Lebombo-Explora Fracture Zones (Revees and de Wit, 2000). From the Cretaceous to the Paleogene (mid-Oligocene), the East African margin was characterized by a period of stability and thermal subsidence (Kent et al., 1971; Salman and Abdula; 1995), which was recorded by deposition of the Kilwa Group in Tanzania (Nicholas et al., 2006; 2007). The passive margin phase was interrupted by neo-rifting and tectonic reactivation: the onset of new mantle circulation beneath the African continent (Ebinger and Sleep; 1998; Moucha and Forte, 2011), known as the African super-swell (Nyblade and Robinson, 1994), evolved into the EARS (Chorowitz, 2005), with synchronous initiation along its western and eastern branches (Roberts et al., 2012). Normal faulting and rifting was widespread along the Tanzanian margin during the Miocene, promoting formation of topographic highs, as Zanzibar, Pemba and Mafia Islands, and lows, such as the coastal basins and the Kerimbas Graben (Kent et al., 1971; Mougenot et al., 1986). Recent studies, however, highlighted the presence of folding and inversion structures on a seismic profile across the channel north of Zanzibar Island (Sii and Underhill, 2015), suggesting that the islands are compressional features associated with fault reactivation and basin inversion.

3.1. Kerimbas Graben and Davie Ridge in the offshore of Tanzania

The EARS consists of a series of tectonic basins bordered by uplifted shoulders, which extend for thousands of kilometres along two main lineaments, called the western and eastern branches (Chorowitz, 2005). The continuation of the eastern branch offshore of Tanzania can be traced along the Pemba and Mafia basins and along the Kerimbas and Lucerna Grabens further to the south (Fig. 1; Mougenot et al., 1988; Franke et al., 2015).

The Kerimbas Graben was firstly recognised by Mougenot et al. (1988) north of the Saint-Lazare Seamount (Fig. 1). A compilation of recently acquired multibeam data highlight that the graben, north of a 12° S, can be divided in three zones based on sea floor morphology and water depth (Figs. 1 and 2). The southern part (zone 1; Fig. 2), between the Saint-Lazare Seamount up to 10° 20’ S, is a 30-40 km wide symmetric graben bounded by ca. 15° steep flanks, and it shows a flat floor lying at a maximum depth of ca. 2900 m, gently dipping to the north (Figs. 1, 2). The western side of the basin runs along the base of the slope in the offshore Rovuma delta while the eastern side corresponds to the Davie Ridge (Fig. 1). A series of channels and gullies cut the western flank and are visible on the sea floor (Fig. 1). The second zone corresponds to a bathymetric sill, located just offshore the main Rovuma Channel between 10° 20’ S and 9° 05’ S (Fig. 1), and it is lying at ca. 2750 metres of water depth (Fig. 2). In this area, the graben shows asymmetric flanks, with a gentler western side up to 1.5°and a 12° dipping eastern side. In the third zone, reaching approximately 8° 40’ S, the graben shows a different morphology with a maximum water depth up to ca. 3500 metres and a maximum width up to 90 km (Figs. 1, 2). In this area, the western flank of the graben partially corresponds to a structural high generated by movement of the Seagap Ridge (Fig. 2; Revees et al., 2016), while the western side corresponds to the northern termination of the Davies Ridge (Fig. 1). A series of arcuate steps are visible on the floor of the graben, likely associated to normal faults developing at the base of the Davie Ridge (see supplementary Figure S1).

The Davie Ridge appears as a bathymetric high roughly extending N-S that dissects the continental slope in the offshore East Africa for more than 1000 km south of 9° S (Mahanjane, 2014; Courgeon et al., 2018). The ridge shows different maximum elevations (calculated as the depth difference between the top of the ridge and the floor

~~of the Kerimbas Graben along a section, see Fig. 2) in the different zones described above (Fig. 2), with an overall decrease in elevation to the north. Heirtzler and Burroughs (1971) when discovering the Davie Ridge described it as a *ridge-like feature*, asymmetric, with a steep western flank (up to 30°) and a gently dipping eastern flank (ca. 0.65° in the offshore Rovuma delta; Fig. 1). Heirtzler and Burroughs (1971) interpreted the ridge as a transform fault resulting from the southward drift of Madagascar relative to the African continent. The continuation of the Davie Ridge north of 9° S, where the ridge does not have a prominent morphological expression on the sea floor (Fig. 1), has been derived by gravimetric and magnetic data showing a series of anomalies, up to 2.5° S (Rabinowitz, 1971; Scrutton, 1978; Coffin and Rabinowitz, 1987). The entire lineament, extending from ca. 20° S to 2.5° S, named the *Davie Fracture Zone* by Scrutton (1978), was interpreted as the bathymetric expression of the transform fault that accommodated southward drift of Madagascar (Scrutton, 1978). A recent study from Klimke and Franke (2016), however, argued the existence of a transform fault extending from northern Mozambique up to Kenya and interpreted the Davie Ridge visible on the bathymetry between 15° S and 9° S (on the eastern side of the Lacerda and Kerimbas grabens) as a rift-flank uplift, originated during the Neogene and probably correlated with the evolution of the EARS in the offshore domain. This interpretation is in agreement with GPS vector data (Calais et al., 2006), and focal mechanisms of recorded earthquakes, showing pure normal faulting with N-NW trending nodal planes and roughly E-W extensional failure (Grimison and Chen, 1988; Yang and Chen, 2010).~~

4. Results

4.1. Stratigraphy of the Davie Ridge

The stratigraphy of the of the Davie Ridge is highlighted in Figure 3, on a seismic profile -oriented NNSW-SSE along the crest of the ridge, and in Figure 4, on a section oriented W-E crossing the eastern side of the Kerimbas Graben. (see Fig. 1 for location). Three laterally-continuous seismic horizons, named H1 to H3, and associated seismic sequences (S1 to S3), were identified based on seismic facies and reflector terminations, mapped throughout the study area, and integrated with all the data available in literature in order to develop a chronological framework for the Davie Ridge. The Tthree sequences, bounded by three key stratigraphic horizons (H1 to H3) plus the sea floor, are recognised. Each sequence, n, named S1 to S3 from shallow deep to deepshallow, shows diagnostic seismic facies, reflection geometries, and RMS amplitude valuesand reflection geometries.

Horizon H1 at the base of sequence S1 presents a laterally variable seismic reflection amplitude (Fig. 3). At places, H1 shows channel-like erosional features that cuts older sediments, as highlighted by the presence of the presence of truncated reflectors (Fig. 4) (add in figure). Overall, Ssequence S1 (, conficonfined between H1 and H2), shows Llow amplitude to transparent reflections, wavy and discontinuous (Fig. 3)., characterize sequence 3 (confined between H2 and H3). When visible, seismic reflections are often wavy to discontinuous (Fig. 3). Overall, S3 S1 shows has low RMS amplitude values (Fig. 4). Higher amplitude reflections, sub-horizonal or shingled, characterize the infill of the erosional features (Fig. 4). . The base of the sequence (H3) corresponds to an erosional surface showing a laterally variable seismic reflection amplitude. Below horizon H3H1, seismic reflections are mainly sub-parallel, with -small lateral changes of seismic amplitude response and overall low RMS amplitude values.

Horizon 2 shows a lateral change in seismic reflection amplitude and a marked erosional character, as highlighted by truncated reflectors belonging to S1. -Sequence S2 (confined between H2 and H3) is dived in two units by horizon J (Figs. 3, 4). Unit S2a (between H2 and J) shows complicated seismic facies, comprising parallel to wavy reflection packages laterally changing from low to high amplitude often accompanied by a change in thickness (Figs. 3, 4). High amplitude reflections characterize the infill of v-shaped (channel-like) erosional depressions (Fig. 4). Overall, S2a shows high RMS amplitude values (Fig. 3). Tabular to lens-shaped deposits showing chaotic to transparent reflections are widespread within S2a and are characterized by low RMS amplitude values (Fig. 4). Unit S2b (between ~~H1~~J and ~~H2~~H3) is characterized by ~~an upper unit (2a) with~~ continuous, high-frequency and low amplitude reflections, mainly with low RMS amplitude values (Figs. 3, 4). The unit presents intervals characterized by higher-amplitude and wavy reflections, ~~wavy or showing a v-shaped basal contact~~ with higher RMS amplitude values. The upper part of S2b is concordant with the overlying sequence S3, and the main difference is a ~~downward~~upward decrease~~increase~~ in the reflection amplitude, as shown by the RMS profile (Fig. 3). Horizon J mainly develops at the top of a series of high-RMS-amplitude reflection packages (Fig. 3). In the high-resolution GLOW seismic profiles, sequence ~~The lower part of S2 (2b) shows a more complicated seismic facies, comprising parallel to wavy reflection packages laterally changing from low to high amplitude often accompanied by a change in thickness (Fig. 3). High amplitude reflections often characterize the infill of v-shaped (channel-like) erosional depressions. Tabular to lens-shaped deposits showing chaotic to transparent reflections are widespread within the lower part of the sequence, and are characterized by low RMS amplitude values.~~

~~S1~~ S3 (between H3 and the sea floor ~~and H1~~) ~~is characterized by~~presents a lower unit (S~~1~~3~~b~~a) mainly characterized by an alternation of parallel and continuous reflections, organized in high- and low-amplitude packages (Fig. 3), ~~.~~ an upper unit (S3~~1~~b~~a~~) showing discontinuous to chaotic seismic reflections with a laterally variable amplitude. ~~, and a lower unit (1b) mainly characterized by an alternation of parallel and continuous reflections, organized in high- and low-amplitude packages (Fig. 3).~~ Overall, ~~S1~~ S3 shows low RMS amplitude values, and a continuous positive reflection defines horizon ~~1~~ 3 (Fig. 3). ~~S2 (between H1 and H2) is characterized by an upper unit (2a) with continuous, high-frequency and low amplitude reflections, mainly with low RMS amplitude values (Fig. 3). In places, the unit presents intervals characterized by higher-amplitude reflections, wavy or showing a v-shaped basal contact with high RMS amplitude values. The upper part of S2 is concordant with the overlying S1, and the main difference is a downward increase in the reflection amplitude, as shown by the RMS. The lower part of S2 (2b) shows a more complicated seismic facies, comprising parallel to wavy reflection packages laterally changing from low to high amplitude often accompanied by a change in thickness (Fig. 3). High amplitude reflections often characterize the infill of v-shaped (channel-like) erosional depressions. Tabular to lens-shaped deposits showing chaotic to transparent reflections are widespread within the lower part of the sequence, and are characterized by low RMS amplitude values. Horizon 2 shows a lateral change in seismic reflection amplitude and a marked erosional character. Low amplitude to transparent reflections characterize sequence 3 (confined between H2 and H3). When visible, seismic reflections are often wavy to discontinuous (Fig. 3). Overall, S3 shows low RMS amplitude values. The base of the sequence (H3) corresponds to an erosional surface showing a laterally variable seismic reflection amplitude. Below horizon H3, seismic reflections are mainly sub-parallel, with small lateral changes of seismic amplitude response and overall low RMS amplitude values.~~

4.2. Super-elevated abandoned canyons on the Davie Ridge

Four giant canyons intersect the crest of the Davie Ridge, approximately running WSW to ENE and named C-1 to C-4 from north to south (Figs. 3, ~~4~~5). C-1 likely represents the landward continuation of the Tanzania Channel, discovered by Bourget et al. (2008) in the Indian Ocean abyssal plain (Fig. 1). ~~Where highlighted by multibeam bathymetry,~~ The~~the~~ canyons are up to 15 km wide and up to 850 m~~etres~~ deep (Fig. ~~4~~5), and their ~~.~~ ~~The~~ thalweg ~~of each canyon~~, measured on the crest of the Davie Ridge, lies at progressively deeper water depths northward, changing from ca. 2,700 m~~eters~~ for C-4 to ca. 3,500 m~~eters~~ of water depth for C-1, which is located about 100 kilometres to the north (Fig. ~~4~~5). While canyons C-4 to C-2 show a U-shaped basal surface, canyon C-1 ~~presents~~ has a~~a~~ flat bottom (Fig. 5)~~topography~~. Seismic profiles highlight that most of the canyons lack a sedimentary infill, except for canyon C-1, showing ca. 0.~~100~~13-~~m~~sec~~eters~~-thick ~~of~~ basal deposits ~~characterized by~~with high-amplitude ~~and~~ parallel reflections (Fig. 5). ~~Due to the northward thinning of S1~~ S3 ~~and S2,~~ While canyon C-4 only cuts across horizon ~~H1~~H3, ~~while~~ ~~canyon~~ C-1 cuts down to ~~horizon H3~~ H1 (Figs. 3, ~~4~~5). Multibeam data acquired along the crest of the Davie Ridge show the morphology of the canyons (Fig. ~~4~~5). Channel C-1 ~~shows~~ presents steep flanks, up to 25°, with the southern one hosting the escarpments of two small landslides (Fig. ~~4~~5, ~~-~~and see supplementary Figure S2). The lack of landslide deposits along the canyon axis suggests that the slumped material was removed by turbidity currents flowing along the canyon, ~~,~~ indicating a recent activity. Direct sampling of the canyon supports this hypothesis, as coarse-grained turbidite deposits are present closely below the sea floor (see supplementary ~~figure~~ Figure ~~S1~~S2). A gentler topography characterizes canyon C-2, showing < 10° dipping flanks (Fig. ~~4~~5). The canyon is cut by a normal fault that creates a step on the sea floor on which sediments, probably transported by bottom currents, ~~may~~ accumulate forming a field of sediment waves (Fig. ~~4~~ 5 and see supplementary

Figure S3). A small sediment drift ~~forms~~ is visible on its northern side and is probably originated by the action of bottom currents as well~~, which can be also related to bottom current activity~~ (Fig. ~~4~~5). The North Atlantic Deep Water (NADW) current is responsible of the deep-water circulation in the western Indian Ocean along the Davie Ridge (van Aken et al., 2004). The orientation of the crest of the sediment waves suggests that bottom currents are directed towards NNE, in agreement with direct observations of the NADW in this area (van Aken et al., 2004). Canyon C-3 is the most noticeable feature on the sea floor as it shows a strong meandering behaviour while crossing the ridge (Fig. ~~4~~5). The canyon presents up to 25° steep flanks, with normal faults on its western side (Fig. ~~4~~5). The multibeam data reveal a small landslide escarpment on the eastern side, with slumped material accumulating on the canyon floor, suggesting that activity of turbidity currents along the canyon was ceased at the time the landslide occurred (Fig. ~~4~~ 5 and see supplementary Figure S4). In addition, the smoothed surface topography of the landslide escarpment and of the deposits suggests that bottom currents probably reworked this area. C-4 is the shallower canyon discovered during the GLOW cruise (Fig. ~~4~~5). The canyon shows a meander-like morphology, with a gentler southern side and steep, up to 20°, northern flank presenting a series of arcuate escarpments, probably generated by sediment failures (Fig. ~~4~~ 5 and see supplementary Figure S5). The lack of a thick pelagic cover on the canyon flanks allowed direct sediment sampling of outcropping strata (~~Box-corer~~ samples GW04 and GW13), providing additional age constraints (Table 1). A 3D view of the area (Fig. ~~5~~6) highlights the geometric relation between the canyons, the Davie Ridge and the Kerimbas Graben. The canyons only incise the Davie Ridge, ~~without~~ and are not visible on the ~~affecting the~~ sea floor of the Kerimbas Graben, which shows a rather flat topography only interrupted by N-S trending fault escarpments (Figs. 4, 6). Indeed, the thalwegs ~~s~~ of the southernmost three canyons are uplifted relatively to the adjacent ~~westward~~ sea floor in the Kerimbas Graben, ~~and the canyons on the Davie Ridge~~implying that the canyons are disconnected from the active slope ~~canyons~~ canyons in the offshore Rovuma and Rufiji River deltas. The presence of N-S fault ~~systems~~ escarpments visible on the multibeam bathymetry and in ~~in~~ cross section on seismic lines ~~data generate topographic steps on the sea floor (supplementary Figure S1),~~ suggests~~ing~~ a recent activity of the offshore branch of the EARS, as discussed also by Franke et al. (2015). This is further confirmed by the location and focal mechanism of recent earthquakes (Grimison and Chen, 1988; Yang and Chen, 2010, and supplementary Figure S1).

4.3. Chronology of the Davie Ridge

The chronology of the Davie Ridge, summarized in Figure 7, was estimated using biostratigraphic information from eight explorations wells, sediment samples, and correlations with published data ~~The correlation of horizons H1 to H3 with dated stratigraphic horizons presented in previous studies~~ (Scrutton, 1978; Mougenot et al., 1986; Coffin and Rabinowitz, 1992;~~ Coffin and Rabinowitz, 1992;~~ McDonough et al., 2013; O' Sullivan, 2013; Franke et al., 2015;~~-~~ Sii and Underhill, 2015; Klimke and Franke, 2016; Sansom, 2018)~~) allowed for the definition of the chronology of the Davie Ridge, summarized in Figure 6. Additional chronological constraints come from the results of the recent hydrocarbon exploration in the area (McDonough et al., 2013; Sii, and Underhill, 2015; Sansom, 2018) and correlaton with DSDP Site 242 (Wade, unpublished)~~. Taking into account the vertical resolution of the seismic data, sediments in proximity of ~~Considering the above:~~ Horizon H1 (Fig. 7) are dated by the Last Occurrence of *Sphenolithus delphix* (top Chattian, ~23.1 Ma; Raffi et al., 2006) and correlates with the base of Ng1 sequence of Sansom (2017), with the top Oligocene reflector (O) of Franke et al. (2015), and with horizon A_1 of Mougenot et al. (1986). H~~h~~orizon H2 is dated by the disappearance of *Helicosphaera perch-nielseniae* and *Sphenolithus heteromorphus* (Serravallian, ~13.5 Ma; Raffi et al., 2006; Boesiger et al., 2017) and correlates with horizon A_{32} of Mougenot et al. (1986). H~~,~~orizon J, for which biostratigraphic information is~~are~~ not available in the wells, most likely corresponds to horizon A_3 of Mougenot et al. (1986), which has been also defined as the late Miocene reflector (LM)~~which has been defined~~ by Franke et al. (2015). H~~ as the late Miocene reflector (LM); H~~orizon ~~H1~~ H3 corresponds to the top of Ng1 sequence of Sansom (2017), base Pliocene (5.3 Ma), and correlates with horizon A_4 of Mougenot et al. (1986).~~, and dates back to the Pliocene;~~ ~~horizon H2 correlates with horizon A3 of Mougenot et al. (1986), which has been defined by Franke et al. (2015) as the late Miocene reflector (LM); horizon H3~~ H1 ~~most likely correlates with A1 of Mougenot et al. (1986) and the top Oligocene reflector (O) of Franke et al. (2015).~~ In addition, the age of ~~Sequence~~ sequence S2, and consequently of horizon ~~H1~~H3, is confirmed by the planktonic foraminifer assemblages~~ of outcropping stratigraphic layers~~sampled on Davie Ridge (Table 1). In detail, box corer sample GW04, recovered from the northern flank of C-1 (Fig. ~~4~~ 5 and supplementary material), represents Zone M14 (age 5.57-6.13 Ma; Wade et al., 2011), while box corer sample GW13, recovered from the southern flank of C-4 (Fig. ~~4~~ 5 and supplementary material), is constrained to Zone PL1 (age 5.54-5.82 Ma; Wade et al., 2011).

5. Discussion and Conclusions

Correlation of seismic data and related attributes allowed evaluation of the deep-water depositional history in the offshore Tanzania. In detail~~,~~ moving upward from ~~Sequence~~

sequence S~~3~~ 1 to ~~Sequence~~ sequence S2, the stratigraphy of the Davie Ridge records~~ed~~ a progressive increase in the accumulation of coarse-grained gravity-driven deposits~~,~~. This is suggested by~~as highlighted by~~ the presence of large turbidite channels, visible in the seismic profiles as v-shaped erosional features hosting high-amplitude reflection packages with shingled reflections (Abreu et al., 2003), ~~-~~and by the overall increase in the RMS amplitude (Figs. 3, ~~6~~7), considered a proxy for sandy sediments (Rijks and Jauffred, 1991; Chen and Sidney, 1997; Brown, 2004). In addition, in the lower part of sequence S2, turbidity current deposits alternate with ~~with debris flow and~~ mass transport deposits, as suggested by the~~ir~~ seismic facies and internal architecture of specific intervals (Fig. 3). ~~(Hampton et al., 1996; Posamentier and Kolla, 2003).~~ Mass transport deposits are the result of gravity-induced remobilization of pre-existing sediments on a submarine slope, and on seismic data are represented by a variety of facies, spanning from chaotic or highly disrupted seismic facies to coherent reflections (Hampton et al., 1996; Posamentier and Kolla, 2003; Frey-Martínez, 2010). The upper part of sequence S1 and the lower unit of ~~part of Sequence~~ sequence S2, which mainly accumulated between the lower and middle~~ is late~~ Miocene~~ in age~~, formed~~accumulated~~ after the establishment of the ~~during the onset of the~~ EARS in Tanzania (Roberts et al., 2012; Sansom, 2017; 2018): at that time, it is possible that topographic uplift in the hinterland increased the progradation of the paleo-Ruvuma and paleo-Rufiji deltas, enhancing deep-water sediment transport and triggering a widespread margin instability, as also discussed in ~~(~~Sansom (~~,~~ 2017; ~~2017~~2018). The presence of turbidite channels and coarse-grained deposits in this stratigraphic interval of the Davie Ridge suggests that sediment sourced from the Tanzanian margin was directly delivered towards the basin, also by means of the giant canyons now present on top of the Davie Ridge. Indeed, considering that the canyons incise the Davie Ridge without reaching horizon

~~H3~~H1, a maximum age for their formation is the age of sequence S2~~, or even younger~~. Moving progressively upward, the upper part of S2 marks a decrease in the activity of turbidite channels, as testified by a reduction of channelized features, which are totally absent in ~~Sequence~~ sequence S~~1~~3. The lack of deposits associated with turbidity currents and debris flows, as highlighted by the seismic data (Figs. 3, ~~4~~5), suggests that the Davie Ridge was at that time a ~~topographic relief~~bathymetric high on the sea floor that acted as barrier for gravity-driven flows ~~triggered~~ originated along the Tanzanian shelf and slope. During deposition of sequence ~~S1~~S3, turbidite channels were still active in the slope area offshore the Rovuma River delta, and further to the north (Liu et al., 2016), and thick turbidite sequences accumulated in the Kerimbas Graben (Franke et al., 2015; Sansom, 2018). Box corer samples and sea floor features visible on the multibeam bathymetry (Fig. ~~4~~ 5 and supplementary material) ~~testify~~ suggest that Canyon C-1, at the northern end of the Davie Ridge, is the only active system and that sedimentation from bottom currents and reduced pelagic and hemiplegic deposition dominates the stratigraphy of the basin outside it.

All these evidences suggest that ~~major~~ the uplift of the Davie Ridge disconnected canyons C-4 to C-2 from their feeder systems, re-routing the sediments delivered into the western Indian Ocean towards the north. Canyon C-1, which is one of the largest deep-water system discovered so far (Fig. ~~7~~8, supplementary S6), represents the termination of a large drainage basin that extends from the Rovuma River to the southern Rufiji River deltas, and that probably connects with the Tanzania Channel about 500 km away towards NE (Bourget et al., 2008). Hence, the Tanzania Channel currently is the main pathway of organic and inorganic particulate matter from the Tanzanian shelf and slope area towards the Indian Ocean abyssal plain. The chronological constraints available show that the topographic deformation of the sea floor associated with the offshore branch of the EARS can be traced back to the ~~late~~ middle-upper Miocene, in agreement with previous studies (Franke et al., 2015). In addition, our results suggest that the tectonic processes driving the uplift of the Davie Ridge that progressively disconnected the deep-water canyons from their feeding systems ~~likely started in the Plio-Quaternary (Fig. 8).~~ are still active today, as demonstrated by the fault displacements visible on the modern sea floor (Figs. 5, 6) and by the ~~The~~ recent recorded earthquakes (supplementary S1), showing a body magnitude M_b up to 6.4 (Grimison and Chen, 1988; Yang and Chen, 2010). ~~demonstrate that the area is still tectonically active, as also indicated by the fault displacements visible on the modern sea floor (Fig. 6). The rapid sea floor deformation triggered by an earthquake may be a potential tsunamogenic source (Kanamori and Kikuchi, 1993), and as a consequence the offshore tectonics of the EARS needs to be taken into account for tsunami hazards assessment along the coastlines of southern Tanzania and Mozambique.~~

This study has two main implications ~~about~~ regarding how the formation of the ~~the meaning of the~~ Davie Ridge relates with~~in~~ the regional geodynamic context and ~~about~~ how the ~~effects~~ tectonics of the offshore branch of the EARS controls the depositional history of the western Indian Ocean. Based on gravimetric and magnetic data, previous studies proposed the existence of a continuation of the Davie Ridge north of 9° S, where it lacks a morphological expression on the sea floor (Coffin and Rabinowitz, 1987; Revees and de Wit, 2000; Revees et al., 2016). With this assumption, the Davie Fracture Zone was correlated up to 2.5° S (Scrutton, 1978; Rabinowitz, 1971; Coffin and Rabinowitz, 1987), and was interpreted as the result of the southward drift of Madagascar with respect to Africa, implying that Madagascar was previously part of the modern Kenya. The ~~inferred Plio-Quaternary~~ Miocene age for the Davie Ridge uplift may suggest that its origin is unrelated with the initial opening of the western Indian

Ocean and with the strike-slip movement of Madagascar, as also proposed by Klimke and Franke (2016). This result would imply the need ~~of~~ for new palaeogeographic models to explain the Mesozoic evolution of the Indian Ocean and the position of Madagascar when attached to Africa. Notwithstanding, it is also possible that the Davie Ridge formed in the response to the recent reactivation of pre-existing Mesozoic tectonic lineaments, but the lack of imaging of the deeper stratigraphic sequences down to the basement does not allow to discuss this point any further.

The discovery of giant and abandoned canyons on the deep-water Davie Ridge highlights that the tectonics of the offshore branch of the EARS has had a profound control on the physiography of the margin and on the transport of sediment and organic matter towards the Indian Ocean. Future studies supported by additional data acquisitions are needed to have a full picture of the modern drainage system and its distal continuation in water depths greater than 4000 metres. There are still outstanding questions regarding ~~Further studies are needed to have a full picture of the modern drainage system and its distal continuation in water depth greater than 4000 metres, and to understand~~ the role of sea floor deformation on bottom current circulation in the western Indian Ocean and ~~.~~the potential of the offshore tectonic activity of the EARS in generating tsunamigenic earthquakes or submarine landslides.

Acknowledgments

The Paleogene GLObal Warming events (GLOW) cruise, onboard of RV Pelagia, was funded by the ESF EUROCORES program~~Netherlands Organisation for Scientific Research (NWO)~~. PNP was supported by NERC UK-IODP grant NE/F523293/1. BW was supported by the Joint Oceanographic Institutions/US Science Support Program.

We thank the Royal Netherlands Institute for Sea Research (NIOZ) for technical and logistic support during and after the cruise. We thank the scientific party for all their support on board the vessel, in particular Niamh O'Sullivan and Chris Nicholas are also thanked. . We are grateful to the Tanzania Petroleum Development Corporation (TPDC), WesternGeco and Schlumberger, Royal Dutch Shell and Shell Tanzania for giving access to the seismic and well data the possibil and allowing the publication of this workity to work and publish the dataset. We would also like to thank , Schlumberger and for providing academic licenses of the seismic interpretation software Petreltheir software (Petrel). PNP was supported by NERC UK-IODP grant NE/F523293/1. BW was supported by the Joint Oceanographic Institutions/US Science Support Program.The Editor, an anonymous reviewer, and Marco Ligi are thanked for their constructive and detailed comments which improved the manuscript significantly. The authors have no conflict of interest to declare.

Data Availability Statement

For more information about the data acquired during the GLOW cruise contact Dick Kroon and Henk de Haas. The bathymetric data are available at doi.org/10.1002/2017GC007274. The other data that support the findings of this study are not publicly available due to privacy restrictions.

References

Abreu, V., Sullivan, M., Pirmez, C., Mohrig, D., 2003. Lateral accretion packages (LAPs): an important reservoir element in deep water sinuous channels. Marine and Petroleum Geology 20, 631-648.

Brown, A.R., 2004. Interpretation of three-dimensional seismic data, 5th edition. AAPG Memoir 42, Tulsa, Oklahoma, pp. 514.

Boesiger, T. M., de Kaenel, E., Bergen, J. A., Browning, E., Blair, S.A., 2017. Oligocene to Pleistocene taxonomy and stratigraphy of the genus Helicosphaera and other placolith taxa in the circum North Atlantic Basin. Journal of Nannoplankton Research 37, 145-175.

Bourget, J., Zaragosi, S., Garlan, T., Gabelotaud, I., Guyomard, P., Dennielou, B., Ellouz-Zimmermann, N., Schneider J.L., 2008. Discovery of a giant deep-sea valley in the Indian Ocean, off eastern Africa: the Tanzania channel. Marine Geology 255, 179-185.

Calais E., Ebinger C.J., Hartnady C., Nocquet J.M., 2006. Kinematics of the East African rift from GPS and earthquake slip vector data. In: Yirgu, G., Ebinger, C.J., Maguire, P.K.H., (Eds.), The Afar Volcanic Province Within the East African Rift System, Geological Society Special Publication 259, pp. 9-22.

Chen C.T., Millero F.J., 1977. Speed of sound in seawater at high pressures. Journal of the Acoustic Society of America 62, 1129-1135.

Chen, Q., Sidney, S., 1997. Seismic attribute technology for reservoir forecasting and monitoring. The Leading Edge 16, 445-448.

Chorowitz, J., 2005. The East African Rift System. Journal African Earth Sciences 43, 379-410.

Coffin, M.F., Rabinowitz, P.D., 1982. A multichannel seismic transect of the Somalian Continental Margin. Offshore Technology Conference, OTC4259, Houston, Texas.

Coffin, M.F., Rabinowitz, P.D., 1987. Reconstruction of Madagascar and Africa: evidence from the Davie Fracture Zone and Western Somali Basin. J. Geophys. Res. 92, 9385-9406.

Coffin, M.F., Rabinowitz, P.D., 1992. The Mesozoic East African and Madagascan conjugate continental margins; stratigraphy and tectonics. In: Watkins, J.S., Feng, Z., McMillen, K.J., (Eds.), Geology and geophysics of continental margins. AAPG Memoir 53, Tulsa, OK, USA, pp. 207-240.

Cohen, A.S., Soreghan, M.J., Scholz, C.A., 1993. Estimating the age of formation of lakes: An example of Lake Tanganyika, East African Rift System. Geology 21, 511-514.

Courgeon, S., Bachèlery, P., Jouet, G., Jorry, S.J., Bou, E., BouDagher-Fadel, M.K., Révillon, S., Camoin, G., Poli, E., 2018. The offshore east African rift system: new insights from the Sakalaves seamounts (Davie Ridge, SW Indian Ocean). Terra Nova 30, 380-388.

Dorschel, D., Jensen, L., Arndt, J.E., Brummer, G.-J., de Haas, H., Fielies, A., Franke, D., Jokat, W., Krocker, R., Kroon, D., Pätzold, J., Schneider, R.R., Spieß, V., Stollhofen, H., Uenzelmann-Neben, G., Watkeys, M., Wiles, E., 2018. The Southwest Indian Ocean Bathymetric Compilation (swIOBC). Geochemistry, Geophysics, Geosystems 19, 968-976.

Ebinger, C.J., Sleep, N., 1998. Cenozoic magmatism throughout East Africa resulting from impact of a single plume. Nature 395, 788-791.

Franke, D., Jokat, W., Ladage, S., Stollhofen, H., Klimke, J., Lutz, R., Mahanjane, E.S., Ehrhardt, A., Schreckenberger, B., 2015. The offshore East African Rift System: structural framework at the toe of a juvenile rift. Tectonics 34, 2086-2104.

Frey-Martínez, J., 2010. 3D seismic interpretation of mass transport deposits: implications for basin analysis and geohazard evaluation. In: Mosher, D.C., Shipp, R.C., Moscardelli, L., Chaytor, J.D., Baxter, C.D.P., Lee, H.J., Urgeles, L., (Eds.), Submarine Mass Movements and Their Consequences. Advances in Natural and Technological Hazards Research 28, 553-568, Springer, Dordrecht.

Goudie, A.S., 2005. The drainage of Africa since the Cretaceous. Geomorphology 67, 437-456.

Grimison, N.L., Chen, W.-P., 1988. Earthquakes in the Davie Ridge-Madagascar region and the southern Nubian-Somalian plate boundary. Journal of Geophysical Research 93, 439-450.

Hampton, M.A., Lee, H.J., Locat, J., 1996. Submarine landslides. Reviews of Geophysics 34, 33-59.

Heirtzler, J.R., Burroughs, R.H., 1971. Madagascar's Paleoposition: New Data from the Mozambique Channel. Science 174, 488-490.

~~Kanamori, H., Kikuchi, M., 1993. The 1992 Nicaragua earthquake: a slow tsunami earthquake associated with subducted sediments. Nature 361, 714-716.~~

Kent, P.E., Hunt, J.A., Johnstone, D.W., 1971. The Geology and Geophysics of Coastal Tanzania. Institute of Geological Sciences Geophysical Paper No. 6, HMSO, London.

Klimke, J., Franke, D., 2016. Gondwana breakup: no evidence for a Davie Fracture Zone offshore northern Mozambique, Tanzania and Kenya. Terra Nova 28, 233-244.

Kroon, D., the Shipboard Scientific Party, 2010. Tropical temperature history during Paleogene Global Warming (GLOW) events. NIOZ Site Survey Cruise Report (R.V. Pelagia cruise number 64PE303), pp. 151.

Leeder, M.R., Jackson, J.A., 1993. The interaction between normal faulting and drainage in active extensional basins, with examples from the western United States and central Greece. Basin Research 5, 79-102.

Liu, X., Rendle-Bühring, R., Henrich, R., 2016. Climate and sea-level controls on turbidity current activity on the Tanzanian upper slope during the last deglaciation and the Holocene. Quaternary Science Reviews 133, 15-27.

Mahanjane, E.S., 2014. The Davie Fracture Zone and adjacent basins in the offshore Mozambique Margin - A new insights for the hydrocarbon potential. Marine and Petroleum Geology 57, 561-571.

Maslin, M.M., Brierley, C.M., Milner, A.M., Shultz, S., Trauth, M.H., Wilson, K.E., 2014. East African climate pulses and early human evolution. Quaternary Science Reviews 101, 1-17.

Macgregor, D., 2015. History of the development of the East African Rift System: A series of interpreted maps through time. Journal of African Earth Sciences 101, 232-252.

McDonough, K-.J., Bouanga, E., Pierard, C., Horn, B., Emmet, P., Gross, J., Danforth, A., Sterne, N., Granath, J., 2013. Wheeler-transformed 2D seismic data yield fan chronostratigraphy of offshore Tanzania. The Leading Edge 32, 162-170.

Moucha, R., Forte, A.M., 2011. Changes in African topography driven by mantle convection. Nature Geoscience 4, 707-712.

Mougenot, D., Recq, M., Virlogeux, P., Lepvrier, C., 1986. Seaward extension of the East African Rift. Nature 321, 599-603.

Nicholas, C.J., Pearson, P.N., Bown, P.R., Dunkley Jones, T., Huber, B.T., Karega, A., Lees, J.A., McMillan, I.K., O'Halloran, A., Singano, J.M., Wade, B.S., 2006. Stratigraphy and sedimentology of the Upper Cretaceous to Paleogene Kilwa Group, southern coastal Tanzania. Journal of African Earth Sciences 45, 431-466.

Nicholas, C.J., Pearson, P.N., McMillan, I.K., Ditchfield, P.W., Singano, J.M., 2007. Structural evolution of southern coastal Tanzania since the Jurassic. Journal of African Earth Sciences 48, 273-297.

Nyblade, A., Robinson, S., 1994. The African superswell. Geophys. Res. Lett. 21, 765-768.

~~Normak, W.R., Carlson, P.R., 2003. Giant submarine canyons: Is size any clue to their importance in the rock record? In: Chan, M.A., Archer, A.W., (Eds.), Extreme depositional environments: Mega end members in geologic time, Geological Society of America Special Paper 370, Boulder, CO, USA, pp.175-190.~~

O' Sullivan, N., 2013. The geological evolution of the Southern Tanzanian continental margin. PhD Thesis, University of Dublin, Trinity College.

Posamentier, H.W., Kolla, V., 2003. Seismic Geomorphology and Stratigraphy of Depositional Elements in Deep-Water Settings. Journal of Sedimentary Research 73, 367-388.

Rabinowitz, P.D., 1971. Gravity anomalies across the East African Continental Margin. J. Geophys. Res. 76, 7107-7117.

Raffi, I., Backman, J., Fornaciari, E., Palike, H., Rio, D., Lourens, L.J., Hilgen, F.J., 2006. A review of calcareous nannofossil astrobiochronology encompassing the past 25 million years. Quaternary Science Reviews 25, 3113-3137.

Reeves, C.V., de Wit, M.J., 2000. Making ends meet in Gondwana: retracing the transforms of the Indian Ocean and reconnecting continental shear zones. Terra Nova 12/6, 272-280.

Reeves, C.V., Teasdale, J.P., Mahanjane, E.S., 2016. Insight into the eastern margin of Africa from a new tectonic model of the Indian Ocean. Geological Society London, Special Publications 431, https://doi.org/10.1144/SP431.12.

Rijks, E.J.H., Jauffred, J.C.E.M., 1991. Seismic interpretation 29; attribute extraction; an important application in any detailed 3-D interpretation study. The Leading Edge 10, 11-19.

Roberts, E.M., Stevens, N.J., O'Connor, P., Dirks, P.H.G.M., Gottfried, M.D., Clyde, W.C., Armstrong, R.A., Kemp, A.I.S., Hemming S., 2012. Initiation of the Western Branch of the East African Rift coeval with the Eastern Branch. Nature Geoscience 5, 289-294.

Salman, G., Abdula, I., 1995. Development of the Mozambique and Ruvuma sedimentary basins, offshore Mozambique. Sedimentary Geology 96, 7-41.

Sansom, P., 2017~~.~~. A new stratigraphic model for Tanzania: Insights from deep water exploration. Presented at the Third EAGE Eastern Africa Petroleum Geoscience Forum, 7–9 November 2017, Maputo, Mozambique~~Turbidites v Contourites: hybrid systems of the Tanzanian margin. PESGB, 16th African E&P Conference, London, UK~~.

Sansom, P., 2018. Hybrid turbidite-contourite systems of the Tanzanian margin. Petroleum Geoscience, 10.1144/petgeo2018-044.

Schumm, S.A., Dumont, J.F., Holbrook, J.M., 2000. Active Tectonics and Alluvial Rivers. Cambridge Univ. Press, 276 pp., Cambridge, UK.

Scrutton, R.A., 1978. Davie fracture zone and the movement of Madagascar. Earth Planet. Sci. Lett. 39, 84-88.

Sepulchre, P., Ramstein, G., Fluteau, F., Schuster M., 2006. Tectonic uplift and Eastern Africa aridification. Science 313, 1419-1423.

Sii, P., Underhill, J.R., 2015. Role of punctuated subsidence and structural inversion in creating the East African Spice Islands. 77th EAGE Conference & Exhibition, IFEMA Madrid, Spain.

~~Simpson, E.S.W., et al., 1974. Phytoplankton stratigraphy, offshore east Africa, Deep Sea Drilling Project Leg 25, in Initial Reports of the Deep Sea Drilling Project, vol. 25, pp. 635-646, U.S. Govt. Print. Off., Washington, D.C.~~

Stankiewicz, J., de Wit, M.J., 2006. A proposed drainage evolution model for central Africa—did the Congo flow east? J. Afr. Earth Sci. 44, 7-84.

van Aken, H.M., Ridderinkhof, H., de Ruijter, W.P.M., 2004. North Atlantic deep water in the south-western Indian Ocean. Deep Sea Research Part I: Oceanographic Research Papers 51, 755-776.

Wade, B.S., Pearson, P.N., Berggren, W.A., Pälike, H., 2011. Review and revision of Cenozoic tropical planktonic foraminiferal biostratigraphy and calibration to the

Geomagnetic Polarity and Astronomical Time Scale. Earth -Science Reviews 104, 111-142.

Yang, Z., Chen, W.-P., 2010. Earthquakes along the East African Rift System: A multiscale, system-wide perspective. Journal of Geophysical Research 115, B12309.

Figure captions

Figure 1. Bathymetry of the western Indian Ocean in the offshore Tanzania and northern Mozambique. Topographic and bathymetric data are ~~freely available and come~~ from GEBCO and the Southwest Indian Ocean Bathymetric Compilation (swIOBC; Dorschel et al., 2018). The ~~bathymetry~~ location of the Tanzania Channel, reported in yellow, is from Bourget et al. (2008).~~ The black dashed lines are the bathymetric cross sections presented in Figure 2. The thick red line is the seismic profile presented in Figure 3.~~

Figure 2. Bathymetric cross sections across the Kerimbas Graben (KG) and the Davie Ridge (DR) north of the Saint-Lazare Seamount (SLS). The black dashed lines in the map mark the ~~are the bathymetric cross sections presented in Figure 2., see~~ location ~~in Figure 1~~. Note the structural high associated to the Seagap Ridge (SR) and the morphological subdivision of the area in~~he Kerimbas Graben~~ in ~~three~~ four zones from south to north ~~(Zone 2 = sill)~~. Blue, green, and red arrows highlight the main fault escarpments, with the location reported in the 3D view of the sea floor with the same colour code.

Figure 3. Seismic line 1, oriented~~-~~ along the Davie Ridge (see location in Fig. 1). Top: Seismic amplitude; Centre: Root Mean Square (RMS) seismic attribute; Bottom: Seismic amplitude with highlighted the main stratigraphic horizons (H1 to H3) and depositional sequences (S1 in ~~green~~red, S2 in blue, S3 in green~~red~~). Note the thalweg of the canyons C-1 to C-4 lies in ~~incisions (C-1 to C-4),~~ progressively deeper towards NNW.

Figure 4. Seismic line 2, oriented W-E across the Kerimbas Graben and the Davie Ridge (see location in Fig. 1).

Figure 5. Seismic profiles across the canyons and high-resolution multibeam bathymetry (location in Fig. 1) of the crest of the Davie Ridge (see supplementary material for close-up views of each canyon). Note the location of the box-corer samples (red dots).

Figure 6~~5~~. 3D view of the Kerimbas Graben and Davie Ridge in the offshore Tanzania.

Figure ~~6~~7. Chronology of the Davie Ridge. 1: Stratigraphic sequences from Sansom (2017); 2: Dated horizons from Mougenot et al. (1986); ~~2~~3: Dated horizons from Franke et al. (2015); ~~3~~4: Age of box corer samples GW04 and GW13 (red bars); ~~4~~5: ~~S~~Seismic horizons of the present study; 6: Extraction of a seismic line across one of the exploration wells used in this study (depth in seconds below the sea floor) with dated stratigraphic sections marked by red rectangles; 7: Interval velocity model of the well; ~~;~~ ~~Extraction of seismic amplitude (5) and RMS (6) with seismic horizons; 7~~8: Stratigraphic sequences and units of this study.~~and main seismic facies.~~

~~Figure 7. Bathymetric cross sections near the shelf-edge of the largest canyons visible on the modern sea floor (in black), modified from Normark and Carlson (2003). Topographic cross section of the Grand Canyon (in brown). Bathymetric cross sections of the deep-water canyons C-1 (the Tanzania Channel) and C-4, in red.~~

Figure 8. Conceptual scheme for the evolution of the study area since the upper Oligocene. Age constraints on key horizons suggest that the uplift of the Davie Ridge (DR) and the formation of the Kerimbas Graben (KG) ~~occurred in the last few millions of years~~started during the middle-upper Miocene. The Seagap Fault (SF) is highlighted in yellow. Note how the deep-water drainage system changed through time in response to the tectonics of the offshore branch of the EARS, from a series of coalescing canyons to a single system, where the Tanzania Channel is the only active conduit.

Sample name	Water depth (m)	Sample depth in the core (cm)	Specimens	Age (Ma)	Biozone
GW04	3,170	29	*Globorotalia plesiotumida*, *Globigerinoides conglobatus* (in the absence of *Globoquadrina dehiscens*, *Globorotalia tumida* and *G. lenguaensis*). Additional marker species include: *Sphaeroidinellopsis seminulina* (in the absence of *Sphaeroidinella* spp.), *Globoturborotalita nepenthes*, *Dentoglobigerina altispira*, *Pulleniatina primalis*, *Globigerinoides extremus*, *Globigerinoides conglobatus*	5.57-6.13	M14
GW13	2,451	33	*Globorotalia tumida*, *Sphaeroidinellopsis seminulina* (in the absence of *Sphaeroidinella*. Additional marker species include: *Menardella limbata*, *Globigerinella siphonifera*, *Globoturborotalia nepenthes*, *Dentoglobigerina altispira*, *Pulleniatina primalis*	4.36-5.57	PL1

Table 1. Microfauna assemblages from box-corer samples GW04 and GW13, and associated chronologies and biozones (see also Wade et al., 2011).

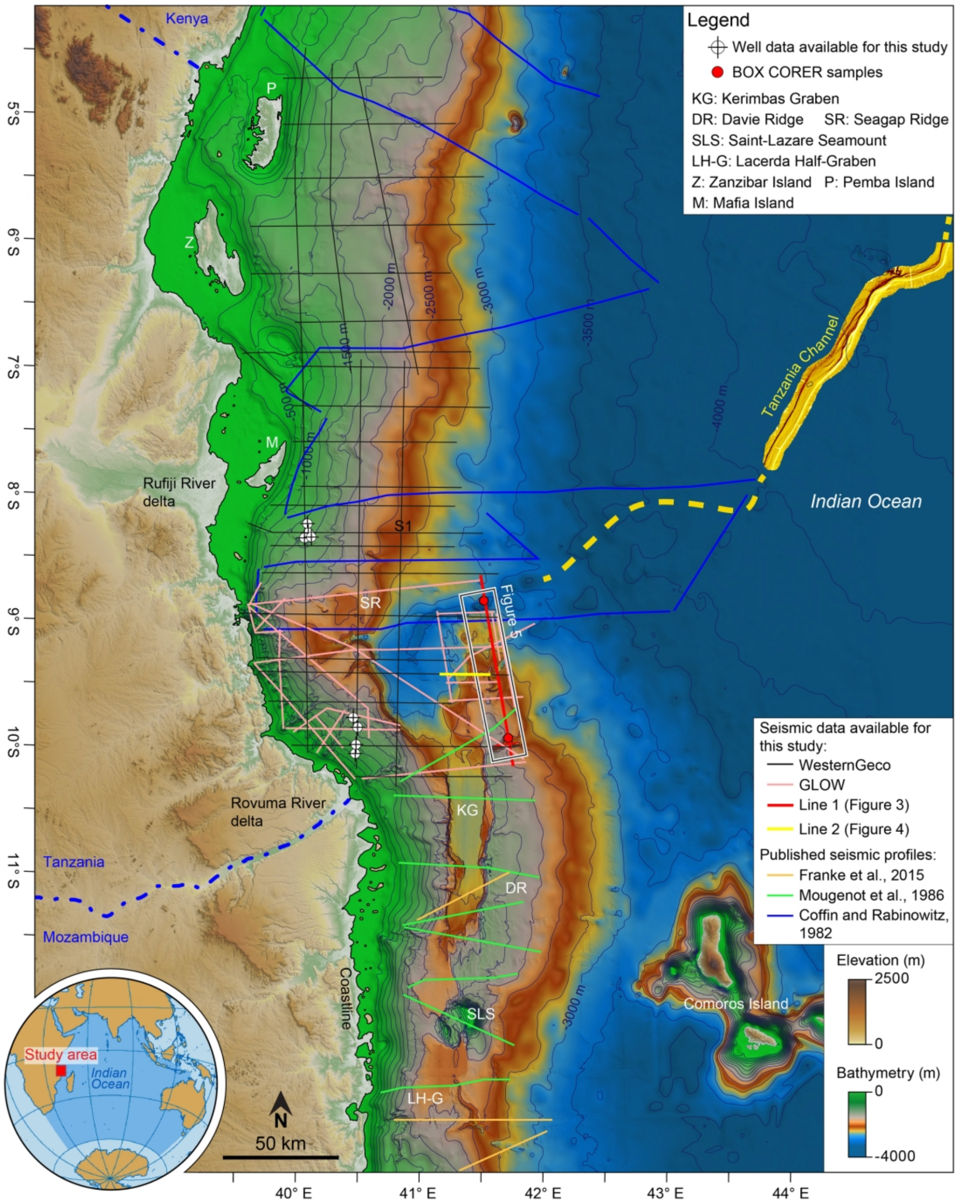

Figure 1 (2-colum size)

179x225mm (300 x 300 DPI)

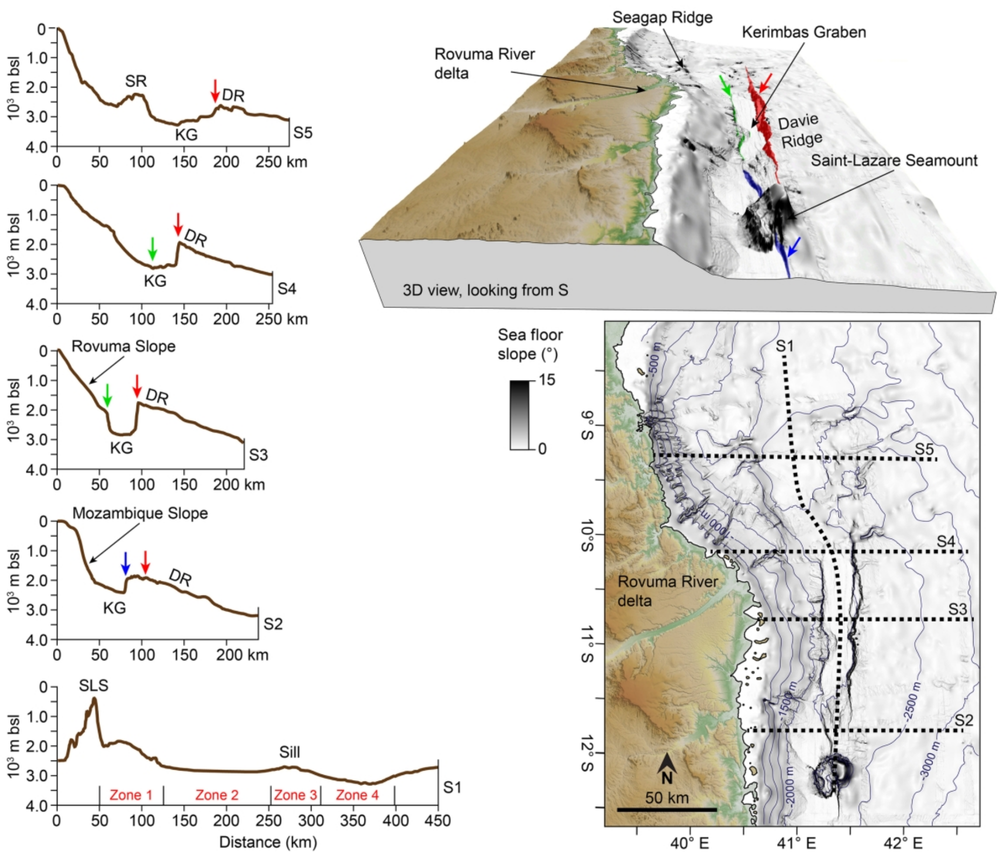

Figure 2 (2-column size)

177x150mm (300 x 300 DPI)

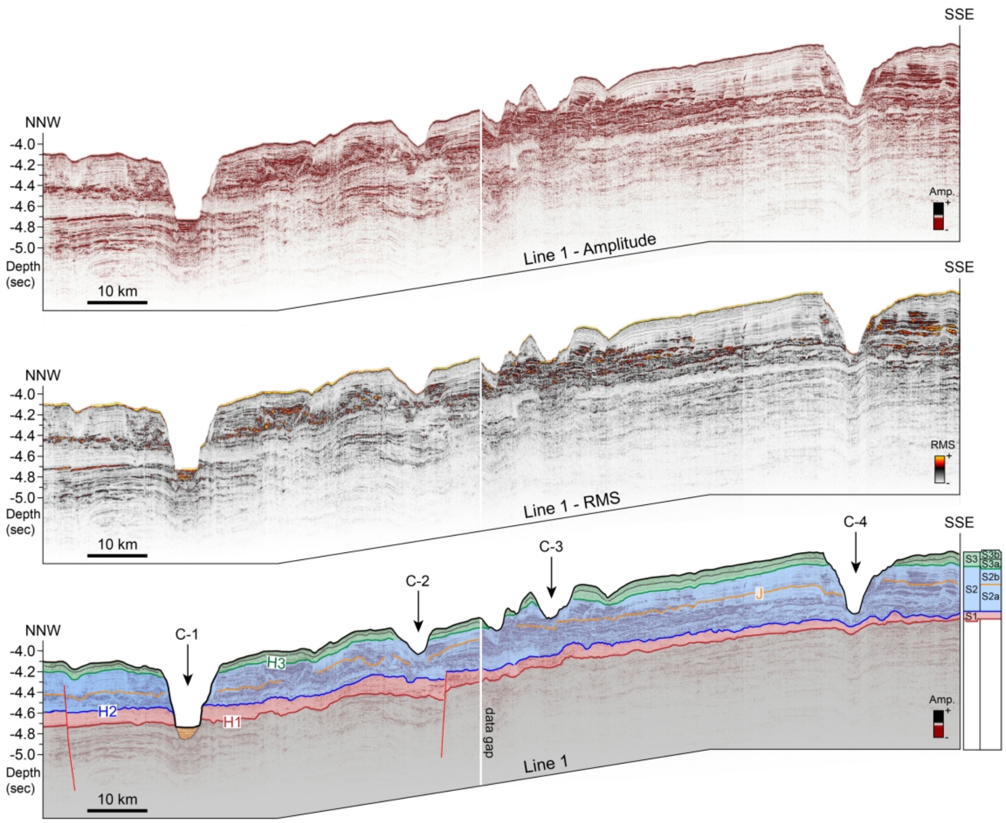

Figure 3 (full page size)

213x174mm (300 x 300 DPI)

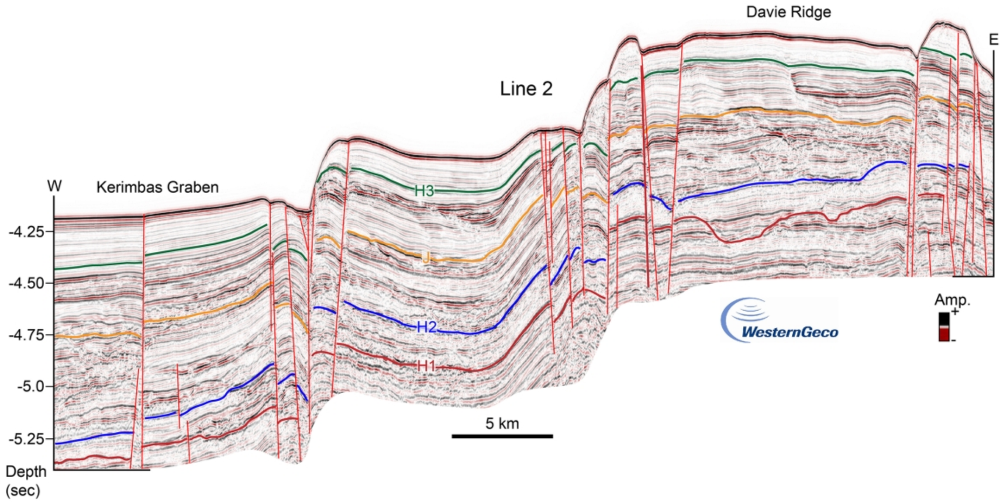

Figure 4 (2-column size)

180x90mm (300 x 300 DPI)

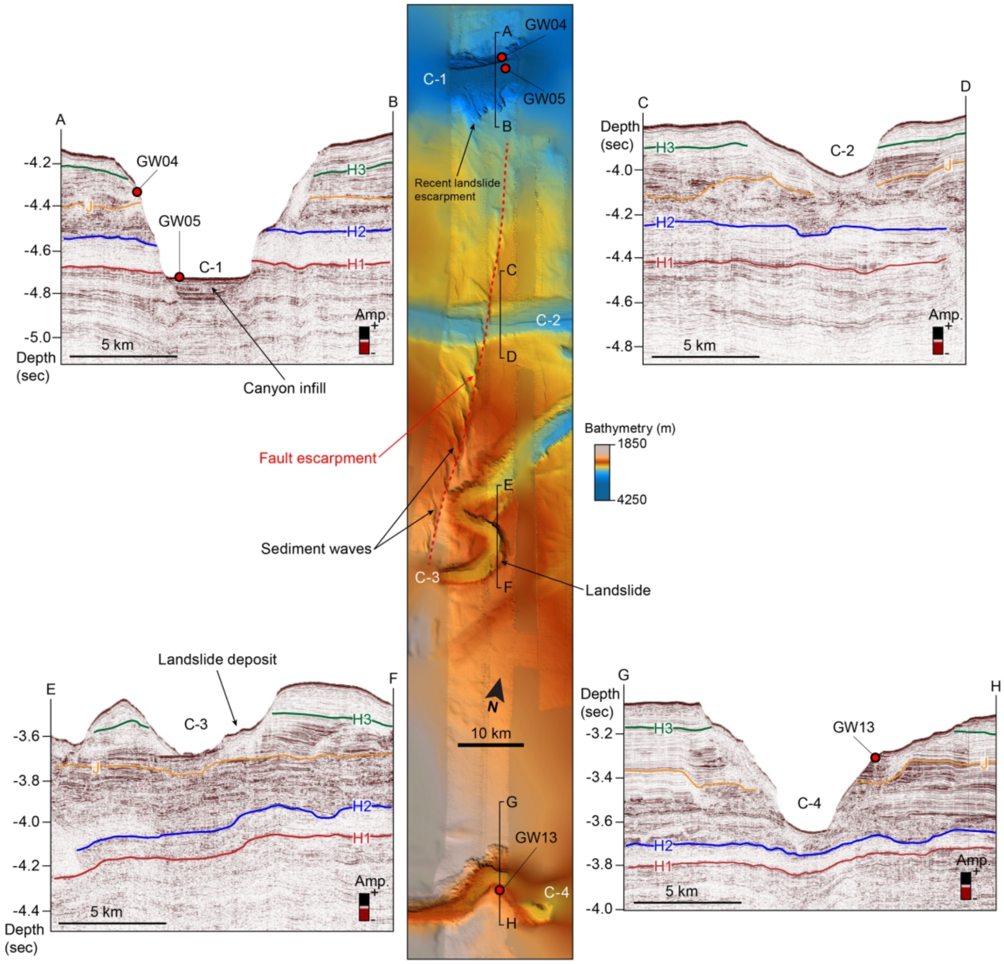

Figure 5 (2-column size)

188x181mm (300 x 300 DPI)

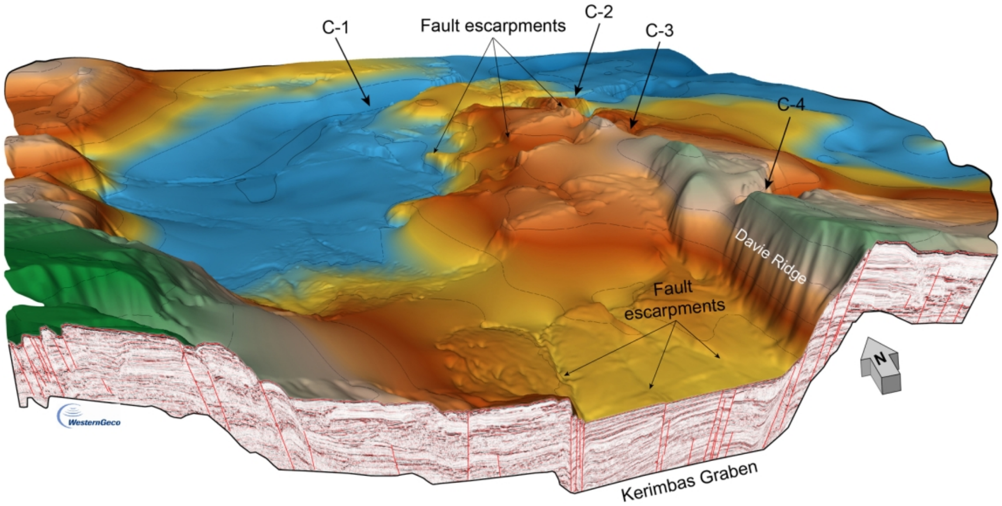

Figure 6 (2-column size)

158x79mm (300 x 300 DPI)

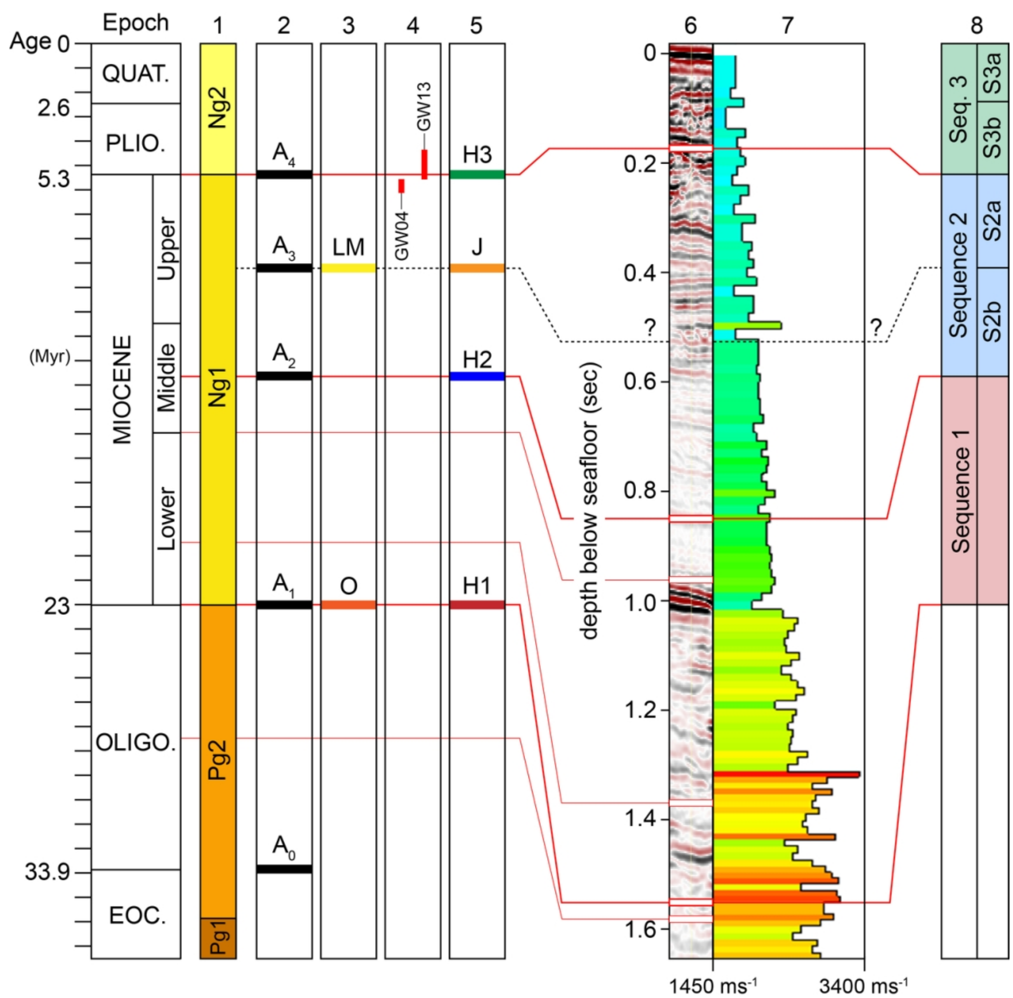

Figure 7 (2-column size)

119x117mm (300 x 300 DPI)

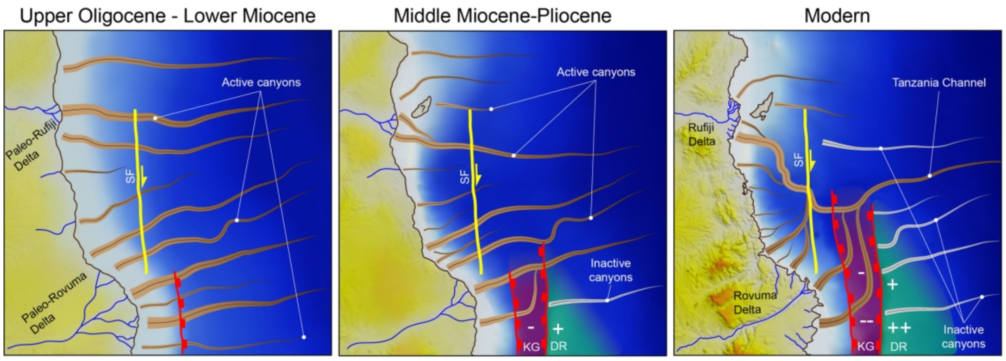

Figure 8 (2-column size)

180x63mm (300 x 300 DPI)